

Economical synthesis of Carbon nanoparticles

A Thesis

presented to

the Faculty of the Graduate School
at the University of Missouri-Columbia

In Partial Fulfillment

of the Requirements for the Degree

Master of Science

by

Charles H. Laber

Dr. Gary A. Baker, Thesis Supervisor

December 2016

The undersigned, appointed by the dean of the Graduate School, have examined the thesis entitled

Economical synthesis of Carbon nanoparticles

presented by Charles Laber,

a candidate for the degree of master of science, and hereby certify that, in their opinion, it is worthy of acceptance.

Professor Gary A. Baker

Professor Shelia N. Baker

Professor Luis Polo-Parada

Acknowledgements

I would like to thank my committee, Dr. Shelia Baker, Dr. Gary A. Baker and Dr. Luis Polo-Parada for their guidance and shared wisdom during my time at the University of Missouri. The training in orienting experiment apparatuses for photos and presentation skills were some of the skills that Dr. Shelia N. Baker shared with me throughout my journey. Dr. Gary A. Baker exposed me to the realm of Nano Chemistry and aided in my development as an independent researcher by guidance through experimental development and synthesis of materials. Also, Dr. Gary A. Baker introduced me to Dr. Luis Polo-Parada who taught me a variety of biological experiments and nurtured my ability to develop and craft apparatuses for experiments. The experience that I gained from everyone will always be remembered and cherished.

Table of Content

Acknowledgments	ii
List of Figures	iv
Chapters	
1. Introduction	1
1.1 Carbon nano structures	1
1.2 Carbon nano quantum dots	3
1.3 Overview	7
2. Domestic Pressure Cooker as an Inexpensive Hydrothermal Vessel	10
2.1 Introduction	11
2.2 Materials and Reagents	13
2.3 Instrumentation	14
2.4 Synthesis of Carbon dots	15
2.5 Quantum yield calculations	16
2.6 Cellular viability and imaging studies	17
2.7 Aqueous metal ion sensing	18
2.8 UV-Vis spectroscopy	20
2.9 Fluorescence spectroscopy	21
2.10 Quantum Yields	23
2.11 Fourier-transform infrared (FTIR) spectroscopy	25
2.12 Transmission electron microscopy (TEM)	27
2.13 Cell viability and fluorescence imaging studies	27
2.14 Conclusion	31
Appendix	
Supporting Information	36

List of Figures

Figure 1.1	5
Figure 1.2	6
Scheme 1.1	13
Figure 2.1	18
Figure 2.2	19
Figure 2.3	21
Figure 2.4	22
Figure 2.5	23
Figure 2.6	25
Figure 2.7	26
Figure 2.8	27
Figure 2.9	28
Figure 2.10	30

Chapter One

Introduction

1.1 Carbon nano structures

One of the core values of a capitalistic market is cost efficiency which is tried and true even in cursed with discovering and developing materials as inexpensive as possible. Now, this is for a multitude of reasons but predominantly research funding programs have begun a movement towards development of field/ micro instrumentation and inexpensive solutions to problems that are seen in medical and environmental fields. Nano particles are one vehicle that allow researchers to pursue the funding for developing solutions to some of the issues concerning the nation today. However, many have and are trying to synthesize nano particles from precious metals such as, gold and silver.¹⁻² These nano particles have been wonderful discoveries and have allowed for enhancement in the fields of electronics, medicine, and environmental safety.³⁻⁵ Although, these achievements are commonly accompanied by concerns of expensive precursors and limited supply. Due to the pitfalls of using precious metals, some have attempted using metals found in great abundance for example, copper, iron, and lead.⁶⁻⁷ Yet, these metals have health concerns for people and wild life. So, one way to overcome the great expenses and the health concerns of metal nano particles is to move to a highly abundant elemental on earth, carbon.

Types of carbon nano structures range from tubes and/or graphene sheets to graphene/carbon quantum dots. Investigators have developed methods to create, grow carbon tubes and sheets with the use of high temperatures and pressures.⁸ Applications of such materials have ranged from gas adsorption, strengthening of building materials and as electron transportation material in solar devices.⁹⁻¹⁰ Graphene quantum dots differ from carbon quantum dots by the starting

Chapter One

material, graphitic core, and surficial functional groups. Requan Ye *et al* have produced a 20 % isolated yield of graphene quantum dots from bituminous coal through an acidic sonication followed by a thermal treatment (100 – 120 °C) for 24 h.¹¹ This process is claimed to synthesize particles ranging in size from 3 to 7 nm with high aqueous solubility.¹¹ To enhance photoluminescent properties of nano particles, some researchers have successfully performed this by the addition heteroatoms into the structure of the particles.

Elements such as, Nitrogen, Sulfur, and Selenium, are a few that have been used to enhance properties.¹²⁻¹⁴ The methods are typically, an addition of a secondary starting material or an additional step after the initial synthesis step. Siwei Yang *et al* used selenium doped graphene quantum dots as reversible fluorescent switches for detection of hydroxyl radicals.¹² These researchers introduced selenium by combining graphene oxide quantum particles (GOQD) with sodium selenide in a Teflon-lined autoclave at 250 °C for 24 h.¹² Approximately 86 % of the GOQDs had incorporated selenium and was confirmed by 3d X-ray photoelectron spectroscopy (XPS) spectrum with peaks at 56.1 eV and 57.0 eV, C-Se and Se-Se, respectively.¹² Nitrogen doped particles have been synthesized by various methods, however one of the more popular methods is the Hummer's.¹³ Yeh and colleagues used a modified Hummer's method to synthesize nitrogen doped GOQDs.¹³ A brief description of Yeh's method is graphite powder, sodium nitrate and concentrated sulfuric acid were combined and mixed in an ice bath. While the mixture was stirring in the ice bath, potassium permanganate was added over a 4 h period to maintain a low temperature.¹³ Deionized water was then to the mixture and the solution was heated to 98 °C for 15 minutes. To conclude the synthesis process, hydrogen peroxide was added to mixture while stirring at room temperature then was dried at 40 °C for one day. To attach nitrogen to the structure, the dried graphene oxide was thermally treated at 500 °C for 3 h in the

Chapter One

presence of ammonia gas. As mentioned previously, the addition of a heteroatom precursor can be utilized to dope particles.¹³ The hydrothermal treatment of Fructose and sulfuric acid is the method that was chosen by Li and coauthors synthesize sulfur doped graphene quantum dots.¹⁴ These sulfur doped particles averaged 5.2 nm in size and have 1 % incorporation of sulfur into the structure, which was confirmed by Fourier transform infrared spectroscopy (FTIR) and Electron energy loss spectroscopy (EELS).¹⁴ The addition of heteroatoms has demonstrated enhancement and tuning of optical properties that could aid researchers in detecting desired analytes and in optoelectronics by diverse electron transition pathways within these graphene nano particles. Although, this type of particle has some of the advantages we are looking for, there is a cousin particle, carbon dot (Cdot) which is typical more amorphous in nature and has higher abundance of heteroatoms due the precursors used to construct this particle.

1.2 Carbon nano quantum dots

Carbon dots (Cdots) are currently a thriving area of research and the focus of this thesis. The inexpensive nature along with tune ability and biocompatibility are the factors that have drawn researcher to this material. Typical characteristics of Cdots include but not limited to: size under 10 nm, excitation wavelength dependent photoluminescence (PL), and great sp^2 carbon characteristics.¹⁵ Also, larger quantities of oxygen are commonly present in Cdots due to the increased carboxyl and other oxygen containing functional groups which aid the aqueous solubility of the nano particles.¹⁵ In 2004, Xu and co-authors stumbled the discovery while attempting to purify single-walled carbon nanotubes that where synthesized by an arc-discharge method.¹⁶ Since their discovery, the synthesis methods have exploded into a wide variety of methods that are simplified into two categories of top-down and bottom-up approaches. The

Chapter One

primary difference between the approaches is that the starting material are either dismantle by harsh treatments such as, arc-discharge, laser-ablation and electrochemical, or smaller precursors are built up into particles by hydrothermal, thermal and microwave approaches.¹⁷

Electrochemical syntheses of Cdots have commonly been accomplished with graphite electrodes but Deng and coworkers reacted an ethanol solution with sodium hydroxide with a three electrode system for approximately for 4 h.¹⁸ During their study, it was observed that electrical potential had slight control over the size distribution with the average particle size doubling from 2 nm to 4 nm when the potential was increased from 3.0 V to 6.0 V. Other approach avenues that have been explored are mixture of saccharides and sodium hydroxide/bicarbonate (room temperature), micro-reactors, and sonochemical.¹⁹⁻²¹ Most researchers have migrated towards bottom-up approaches except when using food or waste materials as precursors.

Thermal and hydrothermal treatments are the greater well-known synthesis routes among the bottom-up approaches. Heating mantels with round-bottom flasks or tube furnaces are the tools researchers that typical resort to for thermal methods. The temperature range is commonly between 200° C – 350° C and 400 ° C – 800° C for heating mantels and tube furnaces, respectively. Benefits of thermal derogation are inexpensive precursors and/or equipment (heating mantel and flasks), along with the ability for large scale production. Reduced temperatures, 90 ° C – 150 ° C, condensed reaction time, 2 h- 8 h, and aqueous matrixes are benefits of hydrothermal practices. However, expenses for this route can be costly due to the apparatus constraints of a programmable oven, Teflon liners and stainless steel autoclaves. Feng et al created Cdots from treating ethylenediamine for 2 h at 90 ° C in a Teflon-lined steel autoclave.²² After purification phases, investigators claim that their procedure yielded 12.1 % quantum yield (QY) when compared to Quinine sulfate and excited at 360 nm.²² Researchers

Chapter One

have used these approaches to synthesize Cdots with capabilities of pH and metals sensors and also functioning photocatalyst and bioimaging agents.²³⁻²⁷ Within my researcher group, we were demonstrated that Cdots could be tailored to increase peroxidase activity of cytochrome *c*.²⁸ Below in Figure 1, the activity of peroxidase with native cytochrome *c* and cytochrome *c* with Cdots can be observed.²⁸

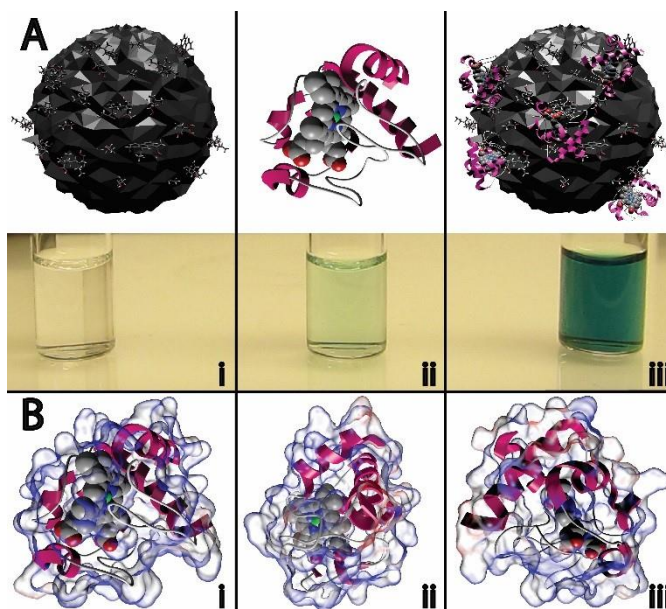


Figure 1.1 (Ai) exhibits that Cdots do not display catalytic activity which is noted by the lack of color. The pale green color in (Aii) is from cytochrome *c* having weak peroxidase activity. When a solution of cytochrome *c* has Cdots combined the peroxidase activity is increased substantially which is caused by the oxidization of leuco-dye 2,2'-azino-bis (3-ethyl-bensothiazline-6-sulphonic, ABTS). Panels (Bi-Biii) are various orientations of the electrostatic calculations performed on cytochrome *c* which illustrates that the protein's surface is positively charged (blue regions) and the majority of positive charges are localized around the heme group.²⁸

The notion of recycling waste has led researchers to plunge into the possibilities of producing using products from waste that is from daily life. The use of food or waste as a precursor for carbon nano materials provides complexity in determining the mechanism of how these materials are fashioned however there are benefits as well. Heteroatom doping is one of the major benefits

Chapter One

of perusing this research along with developing recycling methods. Frying oil and coffee grounds are just a few of the waste materials that have been explored and where successful in producing Cdots.^{25, 26} One material that was utilized as a precursor that was simply overlooked by most was urine. Essner *et al* thermally derogated urine over a 12 h period to produce Cdots which proved to be useful as metal sensors and bioimaging agents.²⁷ In Figure 1.2, merged micrographs of mice embryonic fibroblasts incubated with Cdots are panels (A) and (B). The cell viability is summarized in panel (C) for the three types of Cdots synthesized.²⁷

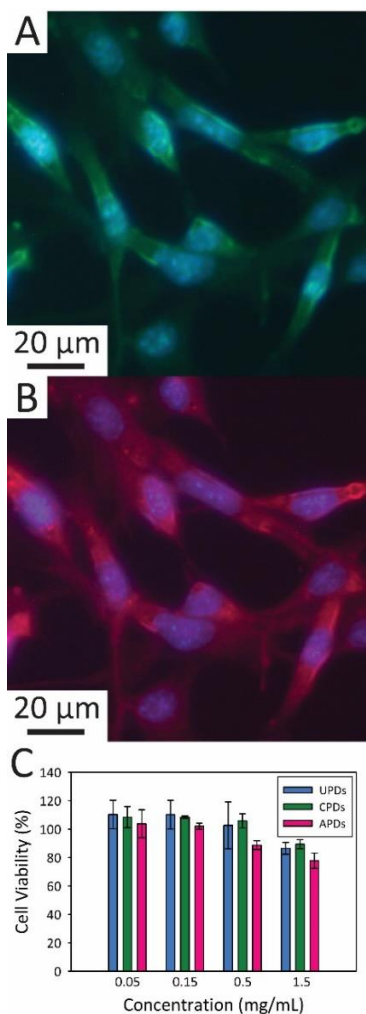


Figure 1.2 Panel (A) and (B) are fluorescence micrographs of Cdot-incubated mice embryonic fibroblast cells with FITC and TRITC filter cube, respectively. The Cdots are located in the

Chapter One

cellular cytoplasm which appear green and red while the nucleus is stained with DAPI. Cell viability studies are summarized in panel (C) indicating that the cells are not harmed by the Cdots up to 1.5 mg/ mL for any of the cdots.²⁷

1.3 Overview

The focus of this thesis research was to develop a carbon dot synthesis method for limited resource institutions. Objectives of the research was to first synthesize particles with a common house item that was space efficient and inexpensive that could be easily accessed by many and to provide that the particles had similar abilities and character as particles found via other routes. To do this a pressure cooker was utilized to emulate the hydrothermal methods within the literature. The particles were characterized by ultra-violet visible spectroscopy, fluorescence spectroscopy, FTIR and transmission electron microscopy. I selective bioimaging agents and metal sensing as application to assess if these particles were comparable the literature.

Chapter One

References

1. M. Brust, M. Walker, D. Bethell, D. J. Schiffrin, R. Whyman, Synthesis of thiol-derivatised gold nanoparticles in a two-phase Liquid-Liquid system, (1994) 801-802.
2. J. Zhu, S. Liu, O. Palchik, Y. Koltypin, A. Gedanken, Shape-Controlled Synthesis of Silver Nanoparticles by Pulse Sonoelectrochemical Methods, *Langmuir*, 16 (2000) 6396-6399.
3. D. I. Gittins, D. Bethell, D. J. Schiffrin, R. J. Nichols, A nanometer-scale electronic switch consisting of a metal cluster and redox-addressable groups, *Nature*, 408 (2000) 67-69.
4. H. L. Lien, W. X. Zhang, Transformation of Chlorinated Methanes by Nanoscale Iron Particles, *J. Environ. Eng.*, 125 (1999) 1042-1047.
5. M. Zhao, R. M. Crooks, Homogeneous Hydrogenation Catalysis with Monodisperse, Dendrimer-Encapsulated Pd and Pt Nanoparticles, *Angew. Chem. Int. Ed.*, 38 (1999) 364- 366.
6. D. W. Zhang, C. H. Chen, J. Zhang, F. Ren, Novel Electrochemical Milling Method To Fabricate Copper Nanoparticles and Nanofibers, *Chem. Mater.* 17 (2005) 5242-5245.
7. R. F. Domingos, M. A. Baalousha, Y. Ju-Nam, M. M. Reid, N. Tufenkji, J. R. Lead, G. G. Leppard, K. J. Wilkinson, Characterizing manufactured nanoparticles in the environment: multimethod determination of particle sizes, *Environ. Sci. Technol.*, 19 (2009) 7277-7284.
8. U. Meier, Strengthening of structures using carbon fibre/epoxy compsites, *Construction and Building*, 9 (1995) 341-351.
9. H. C. Schniepp, J. L. Li, M. J. McAllister, H. Sai, M. Herrera-Alonso, D. H. Adamson, R. K. Prud'homme, R. Car, D. A. Saville, I. A. Aksay, Functionalized Single Graphene Sheets Derived from Splitting Graphite Oxide, 17 (2006) 8535-8539.
10. J. D. Roy-Mayhew, G. Boschloo, A. Hagfeldt, I. A. Aksay, Functionalized Graphene Sheets as a Versatile Replacement for Plantium in Dye-Snesitized Solar Cells, 4 (2012) 2794-2800.
11. R. Ye, C. Xian, J. Lin, Z. Peng, K. Huang, Z. Yan, N.G.P. Cook, E.L.G. Samuel, C. Hwang, G. Ruan, G. Ceriotti, A.O. Ragji, A.A. Marti, J.M. Tour, Coal as an abundant source of graphene quantum dots, *Nature Communications*.4 (2013) 2943.
12. S. Yang, J.Sun, P. He, X. Deng, Z. Wang, C. Hu, G. Ding, X. Xie, Selenium Doped Graphene Quantum Dots as an Ultrasensitive Redox Fluorescent Swith, *Chem. Mater.* 27 (2015) 2004-2011.
13. T.F. Yeh, C.Y. Teng, S.J. Chen, H. Teng, Nitrogen-Doped Graphene Oxide Quantum Dots as Photocatalysts for Overall Water-Splitting under Visible Light Illumination, *Adv. Mater.* 26 (2014) 3297-3303
14. X. Li, S.P. Lau, L. Tang, R. Ji, P. Yang, Sulphur doping: a facile approach to tune the electronic structure and optical properties of graphene quantum dots, *Nanoscale*. 6 (2014) 5323-5328.
15. S.N. Baker, G.A. Baker, Luminescent carbon nanodots: Emergent nanolights, *Angew. Chem. Int. Ed.* 49 (2010) 6726-6744.
16. X. Y. Xu, R. Ray, Y. L. Gu, H. J. Ploehn, L. Gearheart, K. Raker, W.A. Scrivens, *J. Am. Chem. Soc.*126 (2004) 12736-12737.

Chapter One

17. J. Wang, C. Cheng, Y. Huang, B. Zheng, H. Yuan, L. Bo, M.W. Zheng, S.Y. Yang, Y. Guo, D. Xiao, A facile large-scale microwave synthesis of highly fluorescent carbon dots from benzenediol isomers, *J. Mater. Chem. C* 2 (2014) 5028-5035.
18. J. Deng, Q. Lu, N. Mi, H. Li, M. Liu, M. Xu, L. Tan, Q. Xie, Y. Zhang, S. Yao, Electrochemical Synthesis of Carbon Nanodots Directly from Alcohols, *Chem. Eur. J.* 20 (2014) 4993-4999.
19. Y. Li, X. Zhong, A. E. Rider, S. A. Furman, K. Ostrikov, Fast, engery-efficient synthesis of luminescent carbon quantum dots, *Green Chem.* 16 (2014) 2566-2570.
20. Y. Lu, L. Zhang, H. Lin, The Use of a Microreactor for Rapid Screening of the Reaction Conditions and Investigation of the Photoluminescence Mechanism of Carbon Dots, *Chem. Eur. J.* 20 (2014) 4246-4250
21. K. Wei, J. Li, Z. Ge, Y. You, H. Xu, Sonochemical synthesis of highly photoluminscent carbon nanodots, *RSC Adv.* 4 (2014) 52230-52234.
22. X. Feng, Y. Zhao, L. Yan, Y. Zhang, Y. He, Y. Yang, X. Liu, Low-Temperature Hydrothermal Synthesis of Green Luminescent Carbon Quantum Dots (CQD), and Optical Properties of Blends of the CQD with Poly(3-hexylthiophene), *Journal of Elec. Materi.* 44 (2015) 3436-3443.
23. X. Qin, S. Liu, W. Lu, H. Li, G. Chang, Y. Zhang, J. Tian, Y. Luo, A. M. Asiri, A. O. Al-Youbi, X. Sun. Submicrometer-scale polyaniline colloidal spheres: photopolymerization preparation using fluorescent carbon nitride dots as a photocatalyst 2 (2012) 711-714.
24. X. Jia, J. Li, E. Wang, One-pot green synthesis of optically pH-sensitive carbon dots with upconversion luminescence, *Nanoscale*, 4 (2012) 5572-5575.
25. Y. Hu, Jing Yang, J. Tian, L. Jia, J. S. Yu., Waster frying oil as a precursor for one-step synthesis of sulfur-doped carbon dots with pH-sensitive photoluminescence, *Carbon* 77 (2014) 755-782
26. C. Jiang, H. Wu, X. Song, X. Ma, J. Wang, M. Tan, Presence of photoluminscent carbon dots in Nescafe[®] original instant coffee: Applications to bioimaging, *Talanta* 127 (2014) 68-74.
27. J. B. Essner, C. H. Laber, S. Ravula, L. Polo-Parada, G. A. Baker, Pee-dots: biocompatible fluorescent carbon dots derived from the upcycling of urine, *Green Chem.* 18 (2016) 243-250.
28. J. B. Essner, C. H. Laber, G. A. Baker, Carbon dot reduced bimetallic nanoparticles: size and surface plasmon resonance tunability for enhanced catalytic applications, *J. Mater. Chem. A* 3 (2015) 16354-16360.

Chapter Two

Domestic Pressure Cooker as Inexpensive Hydrothermal Vessel

Abstract

A simple and eco-friendly approach that employs a domestic pressure cooker as an inexpensive hydrothermal reactor for the batch synthesis of water-soluble, photoluminescent nanoscale carbon dots derived from benign and cheap commercial starting materials. The resulting carbon nanodots, which consist primarily of hydrophile-decorated amorphous carbon and boast bright, stable, excitation wavelength-dependent fluorescence, were shown to be viable cellular imaging agents for mice embryonic fibroblast cells, displaying little or no cytotoxicity for carbon dot concentrations up to 0.667 mg/mL. In addition, the carbon dots proved useful as nanoprobe for the fluorescence-based detection of environmentally-relevant heavy metal ions such as Cu^{2+} , displaying detection limits below 6 μM , sufficient to determine potable water safety (20 μM is the limit for safe drinking water set by the U.S. Environmental Protection Agency). More generally, these results highlight the utility of a household pressure cooker as a cost-effective hydrothermal vessel relevant to nanocarbon synthesis, opening other possibilities for nano synthesis, particularly in resource-limited settings, educational venues, and the classroom itself.

Chapter Two

2.1 Introduction

The carbon dot (Cdot), the latest nanoscale carbon and cousin to the fullerenes, graphenes, nanotubes, nanodiamonds and nanooxions, has recently emerged as a promising fluorescent nanomaterial that offers attractive, tuneable, and eco-friendly properties (e.g., biocompatibility, inertness, low cytotoxicity),¹⁻³ in comparison to conventional quantum dots made from semiconductor materials such as CdX (X = S, Se, Te). Due to these appealing properties, research exploring various synthetic pathways employing a wide array of means and a wealth of carbon sources has recently witnessed an explosion. These synthetic approaches are generally lumped into two categories: top-down versus bottom-up approaches. Top-down approaches, examples of which include arc discharge,⁴ laser ablation,⁵ and electrochemical oxidation,⁶⁻⁸ involve the cleavage of macroscale carbon sources into smaller carbon “bits”, eventually reaching nanoscale dimensions (i.e., Cdots). On the contrary, bottom-up approaches, such as thermal combustion,^{9,10} templated synthesis,¹¹ microwave synthesis,¹² and hydrothermal techniques,¹³ consist of assembling Cdots, essentially in an atom-by-atom or molecule-by-molecule manner, from carbon-containing molecular precursors. Despite the potentially green nature of Cdots, a substantial portion of these historical synthetic approaches involve the application of high temperatures, acidic/alkaline conditions, expensive (unsustainable) precursors, and/or extensive pre- and post- treatments that do not embrace the principles of green chemistry. Due to these shortcomings, low temperature thermal and hydrothermal approaches using sustainable carbon sources (including low- and negatively-valued wastes, an extreme example of which is human urine¹⁴) as well as syntheses that do not require ensuing functionalization steps have been developed.¹⁵⁻¹⁹ For example, the use of a commercial induction coil heater for the low-temperature thermal synthesis of highly fluorescent Cdots was recently presented.²⁰ Hydrothermal carbonization in particular has been applied to a

Chapter Two

wide range of plant-derived wastes such as spent coffee grounds,²¹ pomelo peel,²² grass,²³ willow bark,²⁴ sweet potatoes,²⁵ giant knotweed rhizome,²⁶ orange juice,²⁷ sweet pepper,²⁸ and waste paper,²⁹ all reported to generate Cdots. While these approaches are substantially greener than many earlier approaches, hydrothermal treatments do require specialized apparatuses (minimally, a Teflon-lined Parr™ bomb in a programmable oven) and are not easily scaled up. Consequently, approaches to the large-volume batch synthesis of Cdots using sustainable strategies remain highly desired.

Essentially a large-scale hydrothermal reactor, albeit with lower temperature and pressure limits, a domestic electric pressure cooker is an intriguing vessel for the simple, cheap, and economical production of nanomaterials. Previously, domestic pressure cookers were shown to be useful for the synthesis of inorganic nanomaterials such as PbS and CdS nanoparticles³⁰ and Cu–In–S/ZnS core/shell quantum dots.³¹ To date, however, there has been no similar demonstration of the utility of a household pressure to prepare nanocarbons. As a proof of concept, the current work adds significantly to the scope of this utility by describing the first implementation of a domestic electric pressure cooker as a facile, economical, one-pot hydrothermal reactor for the batch synthesis of fluorescent nanoscale Cdots. Scheme 1 presents an overview of the pressure cooker synthesis employed in this work. The resulting hydrophilic Cdots possess photophysical properties akin to previously-reported Cdots, including excitation wavelength-dependent fluorescence. As we will show, the pressure cooker-synthesized Cdots function as useful, non-toxic nanoscale labels and sensitive nanoprobe in cellular imaging applications and for the quenchometric sensing of pertinent heavy metal ion contaminants such as Cu²⁺. A distinct outcome of this research is that it allows those in resource-limited settings to contribute meaningfully to the development of novel nanocarbons, including carbon dots, without incurring

Chapter Two

significant startup costs. For instance, the pressure cooker employed here was purchased from a local department store for under US\$100. In contrast, the required equipment for performing a standard hydrothermal reaction (i.e., stainless steel Parr™ bomb with PTFE cups and a programmable oven) will incur a cost of at least US\$3,000, and often significantly more.



Scheme 1.1 A domestic electric pressure cooker operating as a hydrothermal reactor for the synthesis of Cdots. The Cdots were synthesized by treating the precursors for twenty consecutive 99-minute cycles under the cooker’s “high pressure” setting. (No specific endorsement is implied or intended by the use of this particular brand of pressure cooker.)

2.2 Materials and Reagents

All experiments were carried out using Ultrapure Millipore water (18.2 M Ω ·cm). Citric acid monohydrate ($\geq 99.5\%$), D(+)-glucosamine hydrochloride ($>99\%$), urea ($\geq 99.5\%$), sulforhodamine B (SRB), fetal bovine serum, cell culture media, phosphate buffer solution (PBS), trichloroacetic acid, acetic acid, potassium bromide (KBr, anhydrous, 99.95% trace

Chapter Two

metals basis), the chloride salts of Ni^{2+} (98%), Hg^{2+} (ACS >99.5%), Sn^{2+} ($\geq 99.995\%$ trace metal basis), and Mn^{2+} (99.99% trace metals basis), and the sulfate salt of Cu^{2+} ($\geq 98.0\%$) were all purchased from Sigma-Aldrich (St. Louis, MO). Polyethylenimine (PEI), both 1.2 kDa (99%) and 10 kDa (99%), was purchased from Polysciences, Inc. The 96-well plates and the chloride salts of Cu^{2+} (lab grade), Fe^{3+} (ACS 97–102%), Sr^{2+} (99+% ACS), Ba^{2+} (>99%), and Ca^{2+} (99.999%) were obtained from Fisher Scientific (Pittsburg, PA). The anhydrous chloride salt of Zn^{2+} (99.95% metals basis) was acquired from Alfa Aesar (Ward Hill, MA). All chemicals were used as received. Dialysis tubing (132105, Spectra/Por 7, 1 kDa molecular weight cut-off, MWCO) was purchased from Spectrum Labs. The electric pressure cooker (Cuisinart model #CPC-600, 6 qt. capacity) employed in this work was purchased from a local department store. Mice embryonic fibroblast (MEF) cells were acquired from colleagues within the Dalton Cardiovascular Research Center.

2.3 Instrumentation

Absorbance spectra and fluorescence data were collected using a Cary Bio 50 UV-Vis spectrophotometer and a Varian Cary Eclipse Fluorimeter, respectively. Fourier-transform infrared spectra were acquired on a Thermo-Nicolet Nexus 670 ESP FT-IR spectrophotometer using KBr pellets. Transmission electron microscopy (TEM) studies were conducted on carbon coated copper grids (Ted Pella, Inc. 01822-F, support films, ultrathin carbon type-A, 400 mesh copper grid) using a FEI Tecnai (F30 G2, Twin) microscope operated at a 300 keV accelerating voltage. Cells were observed and photographed using an inverted microscope Olympus X-71 with Normanski and fluorescence optics using 4, 10, 20 and 40x lenses and a black and white (Qimaging Retiga EXi) or color (AxioCam MRc5, Carl Zeiss) camera.

Chapter Two

2.4 Synthesis of Carbon Dots

For the hydrothermal pressure cooker synthesis of Cdots, citric acid (CA) and glucosamine (GA) were selected as carbon sources, while polyethylenimine (PEI) and urea (U) were employed as N-doping/passivating agents. These precursors were chosen for several reasons: 1) they are benign and sustainable; 2) they are commercially available in pure form; 3) they are inexpensive; and 4) they contain carboxyl, hydroxyl, and amine functionalities expected to produce highly water-soluble carbon dots. The carboxyl/hydroxyl and amine components are essential as the pressure and temperature conditions within the pressure cooker vessel do not reach a critical level to decompose the carbon precursors but instead engage Maillard-like condensation/amination reactions to generate N-doped Cdots. With this in mind, the following precursor combinations were reacted in our pressure cooker: CA + 10 kDa PEI, CA + 1.2 kDa PEI, and CA + urea. The resulting products are designated CA-PEI₁₀, CA-PEI_{1.2}, and CA-U derived Cdots, respectively. Since GA contains *both* amine and carboxyl/hydroxyl functionalities, we reasoned that it could simultaneously function as both carbon source and self-doping/passivating agent, so GA was tested alone. In a typical synthesis, 10 g of the Cdot precursor (e.g., 5 g each of a carbon and amine source) was dissolved in 0.5 L (2 cups) of 18 MΩ·cm deionized water and then hydrothermally treated on the “high pressure” setting of the pressure cooker for twenty consecutive 99-minute treatments, relieving the pressure (over a 3-5 minute period) after every third treatment to add additional water, as to maintain a constant total volume of ~0.5 L. Interestingly, in the case of the GA-derived Cdots, only ten consecutive treatments were required to obtain the desired product, pointing to the merits of a “single-source” precursor for hydrothermal Cdot synthesis. Upon completion of the hydrothermal treatment, rotatory evaporation reduced the sample volume. The as-synthesized Cdot solutions

Chapter Two

were purified using centrifugation (5000 rpm, 30 min) to remove any solids followed by dialysis (1 kDa MWCO cellulose membrane) to eliminate unreacted carbon source molecules. The dialysis was conducted at room temperature for 48 h against 1.5 L of water, replenishing the dialysate after 24 h of dialysis. The final product was lyophilized and stored at 4 °C until needed.

Although the pressure and temperature within the pressure cooker were not monitored *in situ*, it is worth noting that the “high pressure” setting of domestic electric pressure cookers typically generates pressures between 10-12 psi above atmospheric pressure with corresponding temperatures of 115-120 °C. The “low pressure” setting is typically associated with pressures between 5-8 psi above ambient, yielding a temperature range of 108-113 °C.

2.5 Quantum yield calculations

Quantum yield values were calculated using the equation listed below with quinine sulfate, coumarin 153, fluorescein, and rhodamine B as reference fluorophores (fluorophore and fluorescence measurement information are summarized in Table S1).

$$QY_S = QY_R \left[\frac{F_S}{F_R} \right] \left[\frac{OD_R}{OD_S} \right] \left[\frac{n_S^2}{n_R^2} \right]$$

In this expression, *R* and *S* denote reference and sample, respectively; *F* is the integrated fluorescence intensity (calculated over the wavelength range of interest); *OD* is the optical density (at the excitation wavelength used in the fluorescent measurements), and *n* indicates the solvent refractive index.

Chapter Two

2.6 Cellular viability and imaging studies

The cell viabilities were evaluated based on the sulforhodamine B (SRB) colorimetric assay, as described in the literature.^{32,33} The SRB assay produces more consistent results for adherent cell cultures showing less variations (standard error of measurement, SEM, or coefficient of variation, CV) over an MTT assay. This cell protein dye-binding assay is based on the measurement of the surviving cells' protein content as an index to determine cell growth, inhibition, and cell viability. For the assay, solutions of freshly isolated mice embryonic fibroblast (MEF) cells ($5-8 \times 10^3$ cells in 100 μ L of culture media) were seeded into each well of a 96-well plate and allowed to adhere to the wells for 24 h at 37 °C in a 10% CO₂ atmosphere. Following incubation, the medium was removed and the cells were washed once with 100 μ L of serum-free medium (DMEM/F12). The cells were then treated with various concentrations (0.0667-6.67 mg/mL) of Cdots in 5% fetal bovine serum (FBS) culture media for 24 h at 37 °C in a 10% CO₂ atmosphere. Phosphate buffered saline (PBS) solution was added to each well to bring the total volume within each well to 300 μ L. After Cdot treatment, the medium was removed and surviving or adherent cells were fixed in situ by adding 100 μ L of PBS and 100 μ L of 50% cold trichloroacetic acid (TCA) followed by an incubation period at 4 °C for 1 h. Lastly, the cells were washed with ice-cold water 5 times, dried, and then stained according to the SRB colorimetric assay protocol. The protocol involves staining the cells using 50 μ L of 4% SRB (in 1 vol% acetic acid solution) for 8 min at room temperature. Any unbound dye was removed by washing the cells five times with cold 1% acetic acid and the stained cells were then dried. The bound dye was solubilized with 150 μ L of 10 mM Tris buffer (pH 7.4) and the absorbance of the solutions was measured at 560 nm using a microplate reader. Each Cdot concentration was tested in triplicate. For the fluorescence imaging studies, freshly

Chapter Two

isolated MEF cells were cultured in a 35 mm glass culture dish in the presence of GA-derived Cdots (0.2 mg/mL). DAPI (2 ng/mL) was then introduced to the Cdot/cell mixture for 24 h. The cells were fixed with a 70% ethanol solution for 10 min and mounted with Prolong-Gold Antifade Mountant (Invitrogen) for imaging.

2.7 Aqueous metal ion sensing

Besides fluorescence bioimaging applications, C-dots have shown promise in the aqueous-phase optical sensing of analytes, particularly various metal ions.^{16,23,26} To further demonstrate the practicality of pressure cooker synthesized C-dots, fluorescence quenching behavior was screened against ten different metal ions: Zn^{2+} , Sr^{2+} , Ba^{2+} , Mn^{2+} , Ca^{2+} , Sn^{2+} , Ni^{2+} , Fe^{3+} , Cu^{2+} , and Hg^{2+} , Figure 2.1.

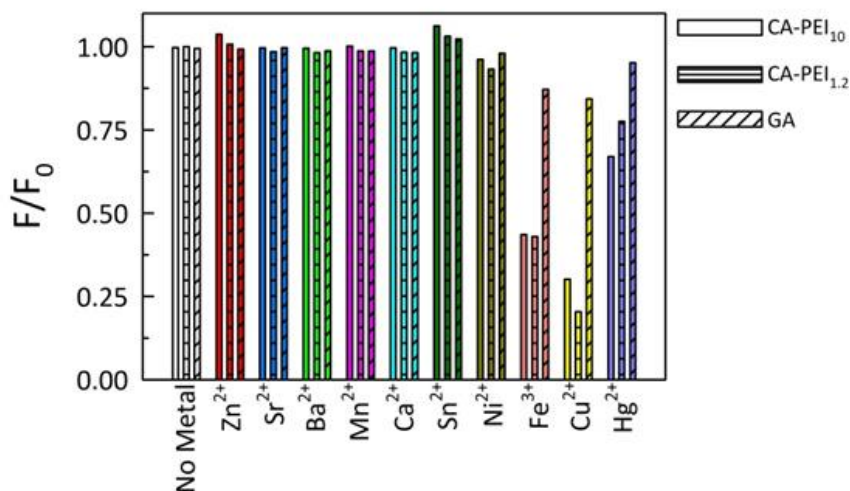


Figure 2.1 Aqueous metal ion screening studies with CA-PEI₁₀, CA-PEI_{1.2}, and GA derived Cdots. Of the ten metal ions tested, Cu^{2+} , Fe^{3+} , and Hg^{2+} ions were the only metals that significantly quenched the C-dot fluorescence, with Hg^{2+} presenting the weakest quenching ability and Cu^{2+} the strongest.

Chapter Two

In general, the three types of C-dots employed in the screening (CA-PEI10, CA-PEI1.2, and GA-derived Cdots) responded in a similar manner to each particular metal ion. For example, Zn^{2+} , Sr^{2+} , Ba^{2+} , Mn^{2+} , Ca^{2+} , Sn^{2+} , and Ni^{2+} metal ions produced no quenching of the Cdot emission whilst Hg^{2+} resulted in relatively weak quenching. Fluorescence from the CA-PEI1.2 and CA-PEI10 Cdots was strongly quenched by Cu^{2+} and Fe^{2+} ions, while Hg^{2+} demonstrated weaker quenching capabilities against PEI derived Cdots. All three of these metals (Fe^{2+} , Cu^{2+} , Hg^{2+}) produced relatively weak quenching of the GA Cdot fluorescence. For all Cdots, Cu^{2+} produced the strongest fluorescence quenching. Therefore, Cu^{2+} titrations were carried out on the CA-PEI10, CA-PEI1.2, and GA-derived Cdots to further clarify the quenching behavior. The corresponding Stern-Volmer plots are provided in Figure 2.2, where F_0 and F represent the fluorescence intensities in the absence and presence of Cu^{2+} , respectively.

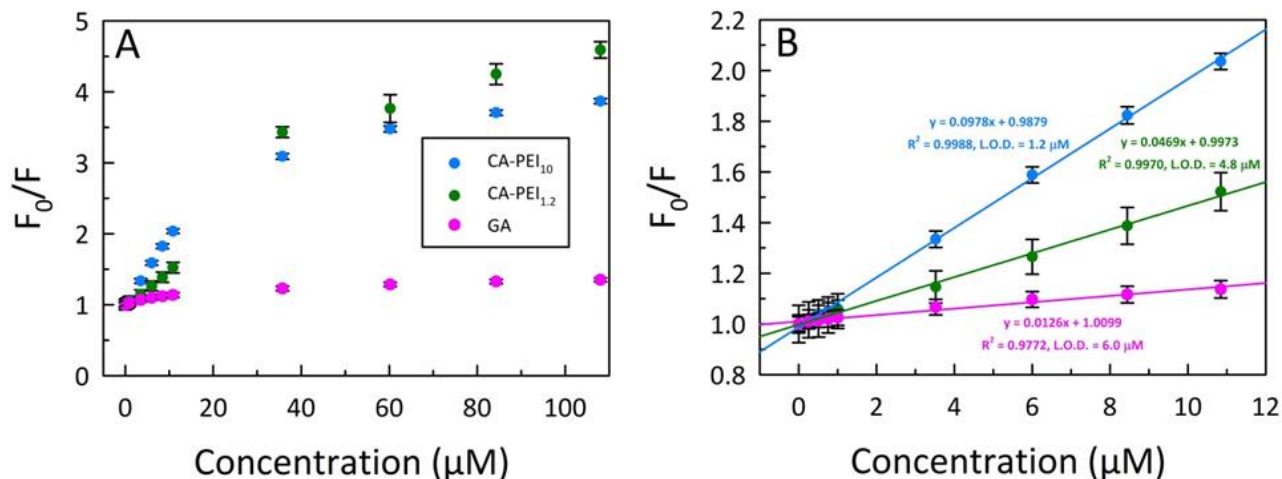


Figure 2.2 (A) Stern-Volmer plots for the Cu^{2+} mediated quenching of the fluorescence from CA-PEI₁₀ (blue), CA-PEI_{1.2} (green), and GA (pink) derived C-dots. (B) Limits of detection (LODs) were assessed over the linear portion in the lower concentration range (0-10 μM). The LODs for all three types of Cdot fall below the US EPA limit of 20 μM for safe drinking water, with the CA-PEI₁₀ Cdots displaying the lowest LOD of 1.2 μM .

Chapter Two

Based on the linear response from 0 to 10 μM Cu^{2+} (Fig. S6B) and following the 3σ convention for limit of detection (LOD), LODs for the various Cdots were calculated as 1.2 μM (CA-PEI10), 4.8 μM (CA-PEI1.2), and 6.0 μM (GA). Despite the fact that these LODs were somewhat higher than that previously reported for Cu^{2+} quenched Cdots,²³ these LODs are still well below the 20 μM limit for safe drinking water established by the U.S. Environmental Protection Agency (EPA),³⁵ making these Cdots convenient tools for assessing water quality.

2.8 UV-Vis spectroscopy

UV-Vis spectroscopy revealed that the various precursor combinations resulted in quite different absorbance features, Figure 2.3. The CA-PEI derived Cdots possessed comparable absorbance profiles showing broad peaks centred at 358 and 354 nm for CA-PEI₁₀ and CA-PEI_{1.2}, respectively. Similarly, the CA-U derived C-dots displayed a broad peak centred at 336 nm but also presented a slight shoulder at approximately 400 nm and an additional peak at 600 nm. On the contrary, the GA-derived Cdots showed increasing absorbance within the UV region and a slight shoulder near 300 nm. The broad absorbance bands from 300-400 nm were attributed to the $n\text{-}\pi^*$ transition of C=O moieties while the strong UV absorbance (<300 nm) was attributed to the $\pi\text{-}\pi^*$ transition of aromatic sp^2 domains (C=C).¹⁹ In addition, the slight bathochromic shift of the broad peaks between 300-400 nm for the PEI incorporated samples could arise from an increased presence of auxochromes such as -OH and -NH groups.

Chapter Two

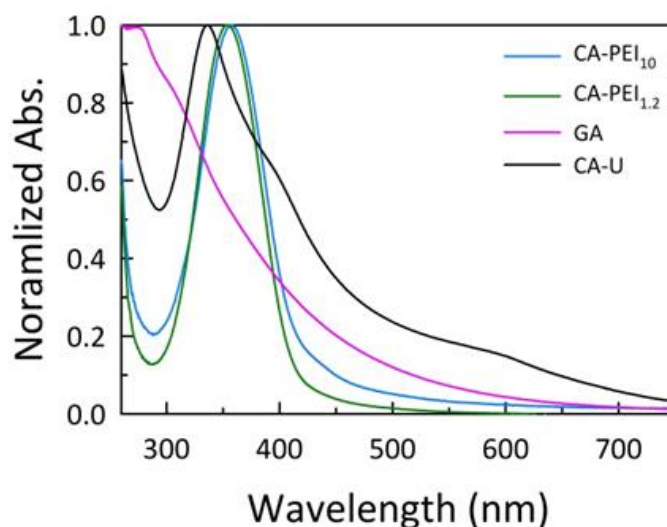


Figure 2.3 Normalized UV-Vis spectra of pressure cooker synthesized Cdots (0.05 mg/mL). CA-PEI₁₀, CA-PEI_{1.2}, and CA-U C-dots displayed similar absorbance profiles with broad peaks centred at 358, 354, and 336 nm for CA-PEI₁₀, CA-PEI_{1.2}, and CA-U Cdots, respectively. In addition, the CA-U Cdots displayed a slight shoulder at approximately 400 nm and an additional peak at 600 nm. Contrary to these Cdots, the GA-derived Cdots possessed a slight shoulder near 300 nm with increasing absorbance upon proceeding from the visible to the UV.

2.9 Fluorescence spectroscopy

Fluorescence spectroscopic analysis reveals that all the pressure cooker synthesized Cdots display a red-edge effect; i.e., the emission wavelength bathochromically shifts as the excitation wavelength increases. The exact origin of a red-edge effect in Cdots is still a somewhat open question but is generally thought to arise from a heterogeneous distribution of particle sizes or chemistries and/or various emissive surface states.^{27,29} Representative fluorescence spectra of the CA-PEI_{1.2} Cdots highlighting the red-edge effect are presented in Figure 2.4. Fluorescence spectra for the other three types of Cdots are provided in Figure 2.5. The peak emission intensities occur at 457, 448, and 454 nm for the CA-PEI₁₀, CA-PEI_{1.2}, and GA-derived Cdots, respectively, all for 350 nm excitation. On the other hand, the CA-U derived Cdots display their highest emission intensity at 460 nm which corresponds to 375 nm excitation.

Chapter Two

The extent of this red-edge effect is shown in the normalized fluorescence emission plots (upper inset plots of Figure 2.4 and Figure 2.5) but can be further illustrated through plots highlighting the dependence of the maximum emission wavelength on the excitation wavelength (lower inset plots, Figure 2.4 and Figure 2.5).

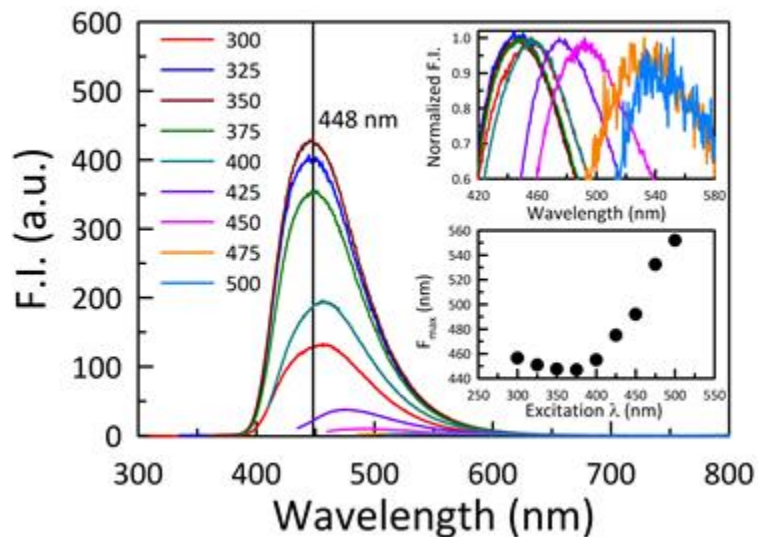


Figure 2.4 Photoluminescence emission spectra of CA-PEI_{1.2} derived Cdots highlighting the red-edge effect. The inset plots further and more clearly illustrate the excitation wavelength-dependent emission. As the excitation wavelength increases, the Cdots display a slight hypsochromic shift until 375 nm excitation, at which point the emission bathochromically shifts in dramatic and essentially linear fashion.

When excited at wavelengths between 300 and 375 nm, the CA-PEI_{1.2} Cdots displayed a slight blue-shift in emission maxima, after which the emission red-shifts in roughly a linear fashion. Similar trends were observed for the other Cdots with the greatest overall red-edge effect arising for the CA-U derived Cdots followed by the CA-PEI_{1.2} derived C-dots. The remaining Cdots displayed similar red-edge effects.

Chapter Two

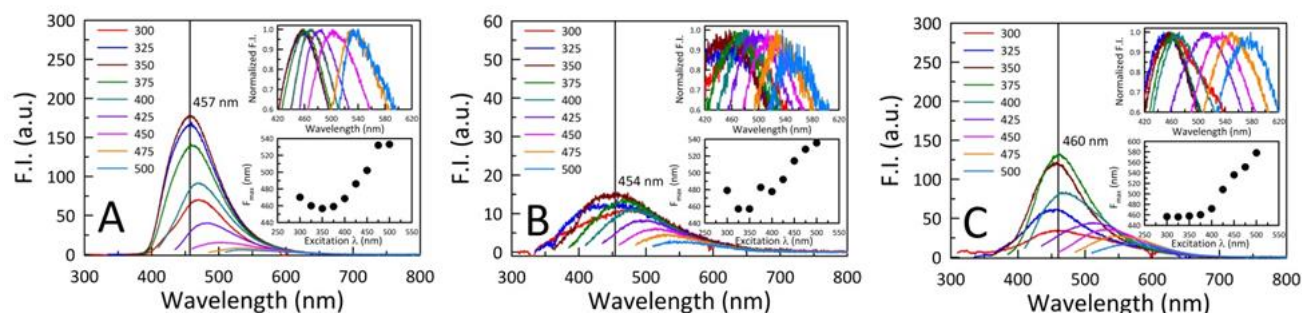


Figure 2.5 Fluorescent emission spectra of (A) CA-PEI10, (B) GA, and (C) CA-U derived Cdots. All Cdote samples displayed a red-edge effect, which is further detailed in the inset plots. In general, upon increasing the excitation wavelength, the fluorescent emission displayed a slight hypsochromic shift, followed by a more substantial bathochromic shift.

While the primary goal of this work was to establish proof of concept for using an inexpensive and widely-available household pressure cooker to synthesize nanocarbons, the difference in emission maxima and the large bathochromic shifts in emission seen underscore the utility of this method for tuning the fluorescent properties of the resultant Cdots simply by variation in the precursor(s) used.

2.10 Quantum yields

Literature reports on hydrothermally-prepared Cdots overwhelmingly report quantum yield (QY) values only at a single wavelength, typically in the UV. For example, certain Cdots were reported to possess QYs up to 38% under 360 nm excitation.¹⁸ In order to make direct comparisons with published values, Cdote QYs were determined at 350 nm using quinine sulfate as the reference fluorophore. Although this is the most commonly employed wavelength/fluorophore combination, reporting QYs at a single wavelength, especially one within the UV range, is not particularly meaningful given the serious limitations of UV light for bioimaging applications where it excites unwanted cellular autofluorescence. In particular, single UV-wavelength QYs provide little insight

Chapter Two

into the fluorescent properties of the red-shifted emission fluorophore sites which offer better prospects for cellular bioimaging. Therefore, we performed a multi-excitation wavelength QY study using three additional dye standards: coumarin 153 (421 nm excitation), fluorescein (470 nm excitation), and rhodamine B (514 nm excitation). All four types of Cdots displayed excitation wavelength-dependent QYs with the general trend of decreasing QY as the excitation wavelength increased (Figure 2.6). In this study, the CA-PEI_{1.2} Cdots resulted in the highest QY (13%) when excited at 350 nm. The two types of dots synthesized using PEI as an amine source follow a similar trend, both showing higher QYs at all wavelengths compared to the GA and CA-U derived Cdots. In addition, the CA-PEI_{1.2} derived Cdots show higher QYs than the CA-PEI₁₀ derived C-dots at 350 and 421 nm excitation wavelengths. This outcome might arise from the 1.2 kDa PEI generating i) smaller, more highly fluorescent dots, or ii) improved Cdot surface passivation, resulting in a greater number of fluorophore sites. The GA and CA-U derived Cdots were found to follow a similar trend to the CA-PEI derived samples, albeit with drastically lower QY values. Interestingly, the QY for the CA-U derived Cdots at 421 nm excitation deviated from this general trend, showing a slight increase in QY relative to 350 nm excitation.

Chapter Two

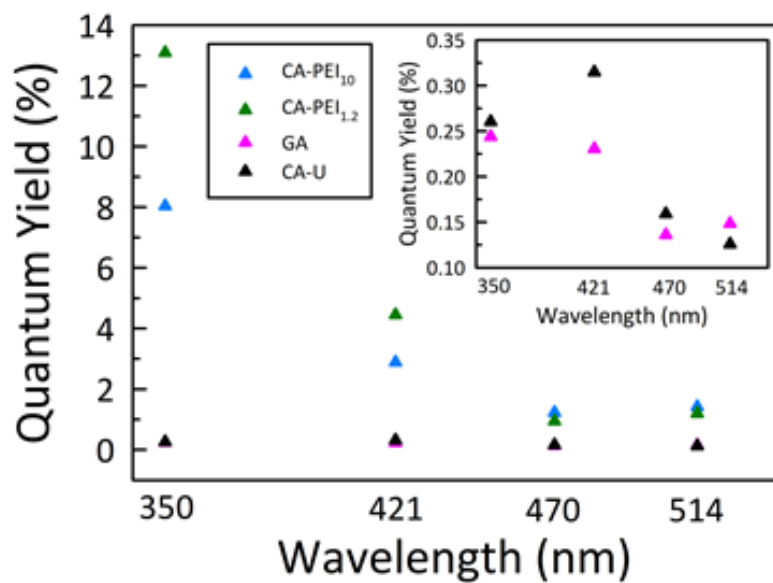


Figure 2.6 Calculated excitation wavelength-dependent QY values for the pressure cooker synthesized Cdots. All samples show a similar general trend of decreasing QY with increasing excitation wavelength. The inset simply provides an expansion of the results for the GA and CA-U derived Cdots.

Chapter Two

2.11 Fourier-transform infrared (FTIR) spectroscopy

Since the surface functionalities of Cdots play pivotal roles in their solubility and photophysical properties, the pressure cooker synthesized Cdots were further characterized with FTIR spectroscopy to reveal the nature of their surface features which can be viewed in figure 2.7.

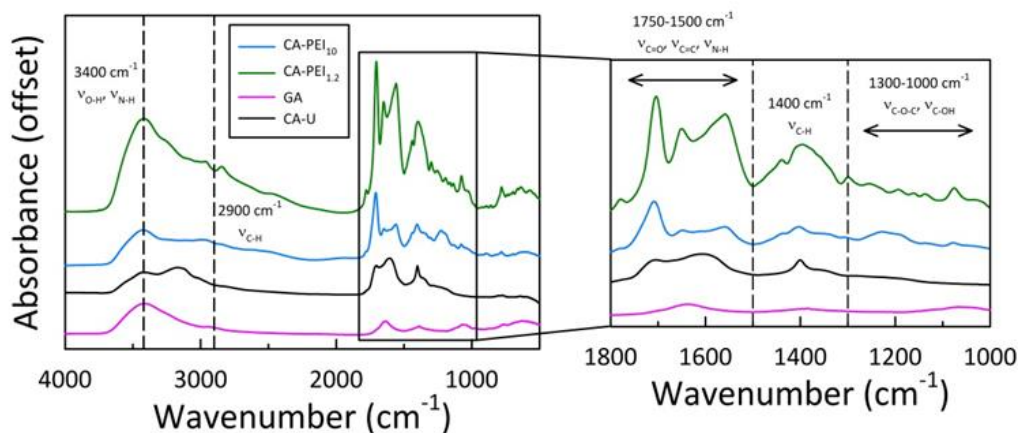


Figure 2.7 FTIR spectra of the pressure cooker synthesized Cdots indicate that the dots contain carboxyl, hydroxyl, ether, ester, amine, and aliphatic carbon moieties on their surfaces. The peak assignments are as follows: 3400 cm^{-1} , stretching vibrations of O–H ($\nu_{\text{O-H}}$) and N–H ($\nu_{\text{N-H}}$); 1700 and 1650 cm^{-1} , stretching vibrations of C=O ($\nu_{\text{C=O}}$); 1650–1550 cm^{-1} , NH/NH₂ deformation ($\nu_{\text{N-H}}$) and skeletal vibrations of aromatic groups ($\nu_{\text{C=C}}$); 1300–1000 cm^{-1} , stretching vibrations of C–O–C and C–OH ($\nu_{\text{C-O-C}}$ and $\nu_{\text{C-OH}}$); 2900 and 1400 cm^{-1} , aliphatic stretches ($\nu_{\text{C-H}}$).

Large, broad absorption bands at approximately 3400 cm^{-1} , assigned to the stretching vibrations of O–H ($\nu_{\text{O-H}}$) and N–H ($\nu_{\text{N-H}}$), were present for all Cdots. Well-defined absorbance bands appeared between 1800 cm^{-1} and 1500 cm^{-1} which were ascribed to the stretching vibrations of C=O ($\nu_{\text{C=O}}$; 1700 and 1650 cm^{-1}), the skeletal vibrations of aromatic groups ($\nu_{\text{C=C}}$; 1650–1550 cm^{-1}), and NH/NH₂ deformation ($\nu_{\text{N-H}}$; 1650 and 1550 cm^{-1}). The various peaks between 1300–1000 cm^{-1} arose from the different stretching modes of carboxylic, ester, ether, and alcohol moieties ($\nu_{\text{C-O-C}}$ and $\nu_{\text{C-OH}}$), while the peaks near 2900 and 1400 cm^{-1} were attributed to aliphatic carbons ($\nu_{\text{C-H}}$).

Chapter Two

The presence of these surface functional groups contributed to the excellent water solubility of the pressure cooker synthesized Cdots and provide evidence for some degree of conjugation.

2.12 Transmission electron microscopy (TEM)

TEM analysis confirmed that consecutive 99-minute treatments of the precursors within the pressure cooker resulted in the formation of Cdots. All the precursor combinations generated particles in the 1-3 nm size range, except for the single-source precursor GA which produced larger particles in the 5-15 nm range (Figure 2.8). Interestingly, the Cdots derived from GA appeared to possess a slight graphitic character as evidenced by the presences of lattice fringes in the TEM images.

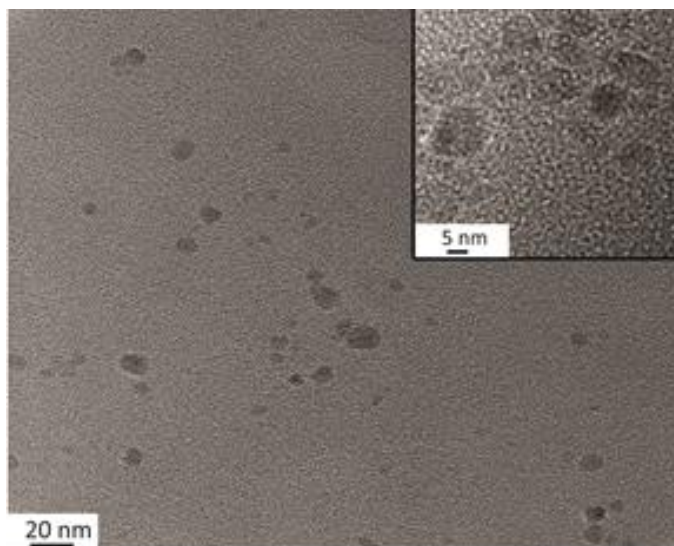


Figure 2.8 Representative TEM image of GA-derived Cdots. The quasi-spherical Cdots ranged in size from 5-15 nm. Interestingly, these Cdots presented lattice fringes indicating they possess a slight graphitic character (inset image).

Chapter Two

2.13 Cell viability and fluorescence imaging studies

Due to their intriguing optical properties and low cytotoxicity, Cdots show promise as novel bioimaging agents for replacing commonly-used (and sometimes toxic) organic dyes.³⁴ To illustrate that Cdots synthesized within a pressure cooker have similar biocompatibility to Cdots synthesized following conventional hydrothermal means, cell viability experiments were conducted on the CA-PEI1.2, CA-PEI10, and GA-derived Cdots (Figure 2.9). The normalized cell viability data indicate that, depending upon the C-dot employed, little to no cell mortality is observed across the tested C-dot concentration range. Both PEI-derived Cdots (CA-PEI10 and CA-PEI1.2) showed a general trend of decreasing cell viability as the Cdot concentration increased, with substantial cell death seen only for concentrations greater than 0.667 or 2.00 mg/mL for CA-PEI10 and CA-PEI1.2 derived dots, respectively.

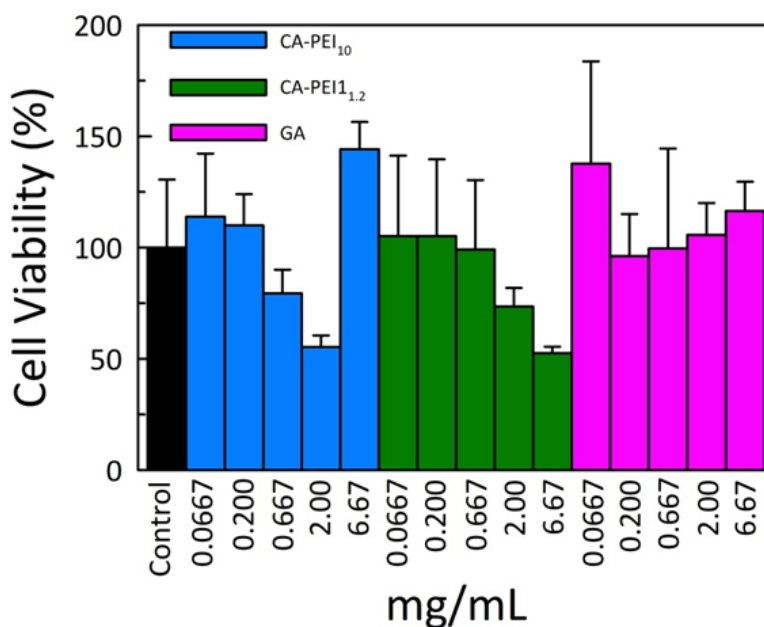


Figure 2.9 Cell viability studies. MEF cells were incubated with CA-PEI10 (blue), CA-PEI1.2 (green), or GA (pink) derived Cdots at concentrations ranging from 0.0667 to 6.67 mg/mL. The PEI containing dots showed similar cell viability trends (decreasing viability) with increasing concentration, although at a concentration of 6.67 mg/mL, the CA-PEI10 Cdots appeared to actually enhance cell growth, a phenomenon deserving further scrutiny. In addition, the GA Cdots exhibited no toxicity to MEF cells across the entire concentration range studied.

Chapter Two

Remarkably, the CA-PEI10 Cdots did not show any cell death at concentrations of 6.67 mg/mL but in fact appeared to enhance cellular growth for reasons not yet fully understood. Contrary to the PEI-derived Cdots, the GA Cdots did not show any cell mortality over the entire concentration range tested, making them prime candidates in bioimaging applications. Despite their modest QY values, the GA-derived Cdots proved to be feasible biolabels for the fluorescent visualization of MEF cells. The fluorescence micrographs of MEF cell cultures incubated with GA-derived Cdots shown in Figure 2.10 confirm that the Cdots can be endocytosed into the cell with the dots distributing throughout the cellular cytoplasm. To provide contrast, the cells were also incubated with 4',6-diamidino-2-phenylindole (DAPI), a nucleus-specific dye that binds strongly to the A-T regions of cellular DNA. Due to the pronounced red-edge effect that these Cdots present, they are compatible with excitation sources spanning the visible spectrum, opening up avenues for multi-color/multiplex detection. To illustrate this, the fluorescence signal was monitored in the blue, green, and orange spectral regions using DAPI, FITC, and TRITC filter sets, respectively. The collected images were then merged to elucidate any labelling differences and potential interaction or competition between DAPI and the Cdots within the cells. These merged images confirm that the GA-derived Cdots were predominately entrapped in vacuoles throughout the cytoplasm (Figure 2.10A: green (FITC) filter set; Figure 2.10B: orange (TRITC) filter set) while the cell nuclei were only stained with DAPI (Figure 2.10A and B: blue). This suggests that there was no competition between the Cdots and DAPI for attaching to the A-T regions of DNA. Overall, these results demonstrate that Cdots prepared in a pressure cooker not only show low cytotoxicity but also have utility for multi-color excitation fluorescence bioimaging.

Chapter Two

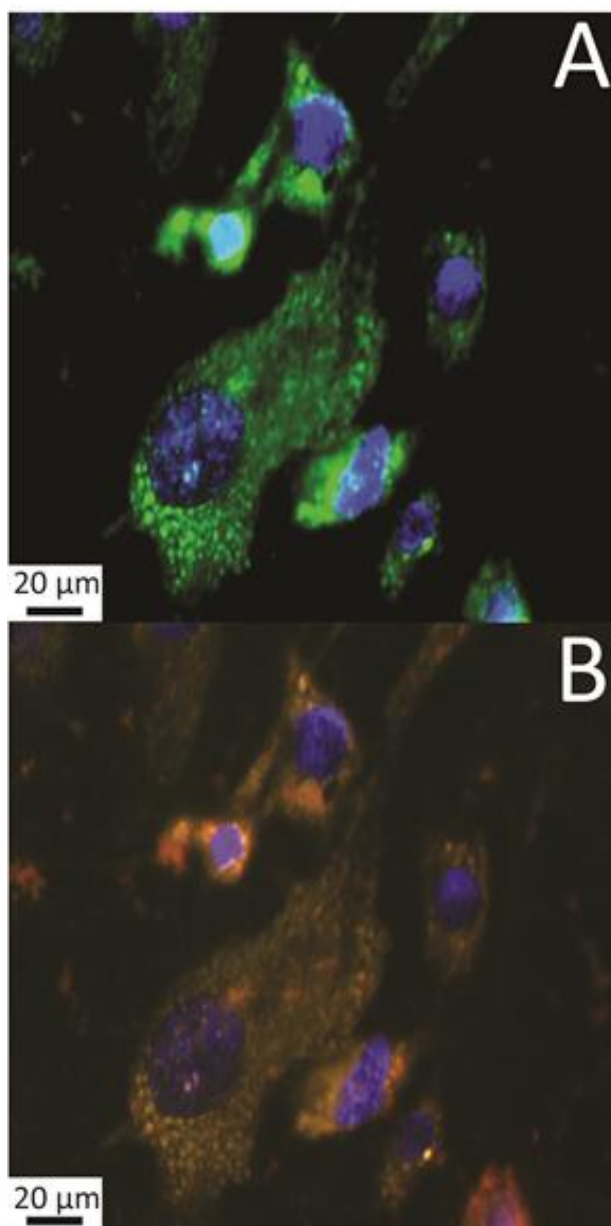


Figure 2.10 Merged fluorescence micrographs of GA-derived C-dot-incubated mice embryonic fibroblast (MEF) cells showing C-dot incorporation into the cellular cytoplasm. The cell images combine the signal from DAPI staining of the nuclear material with the C-dot signal collected through either a (A) FITC or (B) TRITC filter cube.

Chapter Two

2.14 Conclusion

In summary, Cdots were successfully synthesized using a facile, one-pot synthetic approach employing an inexpensive domestic pressure cooker as a soft hydrothermal reactor. The resulting hydrophilic amorphous carbon nanodots displayed bright and stable fluorescence and showed excitation wavelength-dependent behavior in terms of both the emission intensities and fluorescence quantum yields. The pressure cooker synthesized Cdots were shown to be non-cytotoxic in nature which, in conjunction with their useful fluorescent properties, afforded effective multi-color cellular imaging agents, with mice embryonic fibroblast cells used for illustration. In addition, fluorescence from these Cdots was quenched by environmentally-relevant heavy metal pollutants, such as Cu^{2+} , with detection limits well below the U.S. EPA mandated 20 μM level set for safe drinking water. Principally, these results underscore a domestic pressure cooker's utility as a cheap and simple hydrothermal vessel for the synthesis of nanocarbons, particularly in resource-strained settings and educational environments (e.g., class demonstrations).

Chapter Two

References

1. S.N. Baker, G.A. Baker, Luminescent carbon nanodots: Emergent nanolights, *Angew. Chem. Int. Ed.* 49 (2010) 6726-6744.
2. H. Li, Z. Kang, Y. Liu, S.-T. Lee, Carbon nanodots: synthesis, properties and applications, *J. Mater. Chem.* 22 (2012) 24230-24253.
3. R.R. Gaddam, S. Kantheti, R. Narayan, K.V.S.N. Raju, Recent developments of camphor based carbon nanomaterial: Their latent applications and future prospects, *Nano-Structures & Nano-Objects* 3 (2015) 1-8.
4. X. Xu, R. Ray, Y. Gu, H.J. Ploehn, L. Gearheart, K. Raker, W.A. Scrivens, Electrophoretic analysis and purification of fluorescent single-walled carbon nanotube fragments, *J. Am. Chem. Soc.* 126 (2004) 12736-12737.
5. S.-L. Hu, K.-Y. Niu, J. Sun, J. Yang, N.-Q. Zhao, X.-W. Du, One-step synthesis of fluorescent carbon nanoparticles by laser irradiation, *J. Mater. Chem.* 19 (2009) 484-488.
6. J. Zhou, C. Booker, R. Li, X. Zhou, T.-K. Sham, X. Sun, Z. Ding, An electrochemical avenue to blue luminescent nanocrystals from multiwalled carbon nanotubes (MWCNTs), *J. Am. Chem. Soc.* 129 (2007) 744-745.
7. L. Zheng, Y. Chi, Y. Dong, J. Lin, B. Wang, Electrochemiluminescence of water-soluble carbon nanocrystals released electrochemically from graphite, *J. Am. Chem. Soc.* 131 (2009) 4564-4565.
8. H. Li, X. He, Z. Kang, H. Huang, Y. Liu, J. Liu, S. Lian, C.H.A. Tsang, X. Yang, S.-T. Lee, Water-soluble fluorescent carbon quantum dots and photocatalyst design, *Angew. Chem. Int. Ed.* 49 (2010) 4430-4434.
9. A.B. Bourlinos, A. Stassinopoulos, D. Anglos, R. Zboril, V. Georgakilas, E.P. Giannelis, Photoluminescent carbogenic dots, *Chem. Mater.* 20 (2008) 4539-4541.
10. J.B. Essner, C.H. Laber, G.A. Baker, Carbon dot reduced bimetallic nanoparticles: size and surface plasmon resonance tunability for enhanced catalytic applications, *J. Mater. Chem. A* 3 (2015) 16354-16360.
11. Y. Yang, D. Wu, S. Han, P. Hu, R. Liu, Bottom-up fabrication of photoluminescent carbon dots with uniform morphology via a soft-hard template approach, *Chem. Commun.* 49 (2013) 4920-4922.
12. S. Qu, X. Wang, Q. Lu, X. Liu, L. Wang, A biocompatible fluorescent ink based on water-soluble luminescent carbon nanodots, *Angew. Chem. Int. Ed.* 51 (2012) 12215-12218.
13. Q.-Q. Shi, Y.-H. Li, Y. Xu, Y. Wang, X.-B. Yin, X.-W. He, Y.-K. Zhang, High-yield and high-solubility nitrogen-doped carbon dots: Formation, fluorescence mechanism and imaging application, *RSC Adv.* 4 (2014) 1563-1566.
14. J.B. Essner, C.H. Laber, S. Ravula, L. Polo-Parada, G.A. Baker, Pee-dots: biocompatible fluorescent carbon dots derived from the upcycling of urine, *Green Chem.* 18 (2016) 243-250.
15. A.B. Bourlinos, A. Stassinopoulos, D. Anglos, R. Zboril, M. Karakassides, E.P. Giannelis, Surface functionalized carbogenic quantum dots, *Small* 4 (2008) 455-458.
16. Y. Guo, Z. Wang, H. Shao, X. Jiang, Hydrothermal synthesis of highly fluorescent carbon nanoparticles from sodium citrate and their use for the detection of mercury ions, *Carbon* 52 (2013) 583-589.

Chapter Two

17. Y. Cui, Z. Hu, C. Zhang, X. Liu, Simultaneously enhancing up-conversion fluorescence and red-shifting down-conversion luminescence of carbon dots by a simple hydrothermal process, *J. Mater. Chem. B* 2 (2014) 6947-6952.
18. Y. Song, S. Zhu, S. Xiang, X. Zhao, J. Zhang, H. Zhang, Y. Fu, B. Yang, Investigation into the fluorescence quenching behaviors and applications of carbon dots, *Nanoscale* 6 (2014) 4676-4682.
19. Z. Yang, M. Xu, Y. Liu, F. He, F. Gao, Y. Su, H. Wei, Y. Zhang, Nitrogen-doped, carbon-rich, highly photoluminescent carbon dots from ammonium citrate, *Nanoscale* 6 (2014) 1890-1895.
20. M.P. Sk, A. Chattopadhyay, Induction coil heater prepared highly fluorescent carbon dots as invisible ink and explosive sensor, *RSC Adv.* 4 (2014) 31994-31999.
21. P.-C. Hsu, Z.-Y. Shih, C.-H. Lee, H.-T. Chang, Synthesis and analytical applications of photoluminescent carbon nanodots, *Green Chem.* 14 (2012) 917-920.
22. W. Lu, X. Qin, S. Liu, G. Chang, Y. Zhang, Y. Luo, A.M. Asiri, A.O. Al-Youbi, X. Sun, Economical, green synthesis of fluorescent carbon nanoparticles and their use as probes for sensitive and selective detection of mercury(II) ions, *Anal. Chem.* 84 (2012) 5351-5357.
23. S. Liu, J. Tian, L. Wang, Y. Zhang, X. Qin, Y. Luo, A.M. Asiri, A.O. Al-Youbi, X. Sun, Hydrothermal treatment of grass: A low-cost, green route to nitrogen-doped, carbon-rich, photoluminescent polymer nanodots as an effective fluorescent sensing platform for label-free detection of Cu(II) ions, *Adv. Mater.* 24 (2012) 2037-2041.
24. X. Qin, W. Lu, A.M. Asiri, A.O. Al-Youbi, X. Sun, Green, low-cost synthesis of photoluminescent carbon dots by hydrothermal treatment of willow bark and their application as an effective photocatalyst for fabricating Au nanoparticles-reduced graphene oxide nanocomposites for glucose detection, *Catal. Sci. Technol.* 3 (2013) 1027-1035.
25. W. Lu, X. Qin, A. Asiri, A. Al-Youbi, X. Sun, Green synthesis of carbon nanodots as an effective fluorescent probe for sensitive and selective detection of mercury(II) ions, *J. Nanopart. Res.* 15 (2012) 1-7.
26. D. Wu, X. Huang, X. Deng, K. Wang, Q. Liu, Preparation of photoluminescent carbon nanodots by traditional Chinese medicine and application as a probe for Hg²⁺, *Anal. Methods* 5 (2013) 3023-3027.
27. S. Sahu, B. Behera, T.K. Maiti, S. Mohapatra, Simple one-step synthesis of highly luminescent carbon dots from orange juice: application as excellent bio-imaging agents, *Chem. Commun.* 48 (2012) 8835-8837.
28. B. Yin, J. Deng, X. Peng, Q. Long, J. Zhao, Q. Lu, Q. Chen, H. Li, H. Tang, Y. Zhang, S. Yao, Green synthesis of carbon dots with down- and up-conversion fluorescent properties for sensitive detection of hypochlorite with a dual-readout assay, *Analyst* 138 (2013) 6551-6557.
29. J. Wei, X. Zhang, Y. Sheng, J. Shen, P. Huang, S. Guo, J. Pan, B. Liu, B. Feng, Simple one-step synthesis of water-soluble fluorescent carbon dots from waste paper, *New J. Chem.* 38 (2014) 906-909.
30. D. Berhanu, K. Govender, D. Smyth-Boyle, M. Archbold, D.P. Halliday, P. O'Brien, A novel soft hydrothermal (SHY) route to crystalline PbS and CdS nanoparticles exhibiting diverse morphologies, *Chem. Commun.* (2006) 4709-4711.

Chapter Two

31. Y. Chen, S. Li, L. Huang, D. Pan, Low-cost and gram-scale synthesis of water-soluble Cu-In-S/ZnS core/shell quantum dots in an electric pressure cooker, *Nanoscale* 6 (2014) 1295-1298.
32. L.V. Rubinstein, R.H. Shoemaker, K.D. Paull, R.M. Simon, S. Tosini, P. Skehan, D.A. Scudiero, A. Monks, M.R. Boyd, Comparison of in vitro anticancer-drug-screening data generated with a tetrazolium assay versus a protein assay against a diverse panel of human tumor cell lines, *J. Natl. Cancer I.* 82 (1990) 1113-1117.
33. P. Skehan, R. Storeng, D. Scudiero, A. Monks, J. McMahon, D. Vistica, J.T. Warren, H. Bokesch, S. Kenney, M.R. Boyd, New colorimetric cytotoxicity assay for anticancer-drug screening, *J. Natl. Cancer I.* 82 (1990) 1107-1112.
34. M. Chen, W. Wang, X. Wu, One-pot green synthesis of water-soluble carbon nanodots with multicolor photoluminescence from polyethylene glycol, *J. Mater. Chem. B* 2 (2014) 3937-3945.
35. U.S. E.P.A., Maximum contaminant level goals and national primary drinking water regulations for lead and copper; final rule., *Fed. Reg.* 56 (1991) 6460

Conclusion

In Conclusion, an inexpensive pressure cooker has proven to be comparable to programmable ovens paired with Teflon autoclaves, which are commonly found in literature. Even though the particles possess the common properties of Carbon dots, this method does produce irregular structure which is observed in figure 2.8. The particles' shape is the most irregular feature by not being completely spherical. Particle size disruption appeared to be greater for this method with precursor dependence. To further this research, exploration of purification/ fractionation of Cdots or the cellular uptake of the Cdots would be viable avenues. Besides the previous options, the investigation of the mechanism of synthesizing Cdots is another direction however, this research would have greater complexity due the vast amount of interactions, synthesis environments and abundance of precursor combinations. The Benefits of exploring purification methods would allow for clarity on if all sizes of Cdots contain the tuneable emission or if size regimes have different properties. As for exploring cellular uptake, the major benefit would be that insight in where the Cdots would accumulate in the cells and if we could direct them into certain areas. Besides directing the Cdots, determining if they can be a multiple cell generation marker could become promising bio imaging agent in cancer research. If Cdots could stay intact during cellular division then there is a chance that the new generation of cells would uptake, then which in turn would allow for a single injection of Cdots verses multiple dye injections.

Appendix

Supporting Information

Table S1. Reference fluorophores used to determine quantum yield (*QY*) values.

Fluorophore	Excitation Wavelength (nm)	Solvent	<i>n</i> ^a	<i>QY</i> (%)	Ref.
Quinine sulfate	350	0.1 M H ₂ SO ₄	1.343	58	[1]
Coumarin 153	421	EtOH	1.366	38	[2]
Fluorescein	470	0.1 M NaOH	1.336	91	[3]
Rhodamine B	514	Water	1.334	31	[4]

^a refractive index.

References

1. J.R. Lakowicz, Principles of Fluorescence Spectroscopy, Springer, 2007.
2. G. Jones, W.R. Jackson, C.Y. Choi, W.R. Bergmark, Solvent effects on emission yield and lifetime for coumarin laser dyes. Requirements for a rotatory decay mechanism, J. Phys. Chem. 89 (1985) 294-300.
3. L. Porrès, A. Holland, L.-O. Pålsson, A. Monkman, C. Kemp, A. Beeby, Absolute measurements of photoluminescence quantum yields of solutions using an integrating sphere, J. Fluoresc. 16 (2006) 267-273.
4. D. Magde, G.E. Rojas, P.G. Seybold, Solvent dependence of the fluorescence lifetimes of xanthene dyes, Photochem. Photobiol. 70 (1999) 737-744.